Langmuir
Article
pubs.acs.org/Langmuir

Controlled Assembly of Janus Nanoparticles

Qiao Xu, Xiongwu Kang, Roberto A. Bogomolni, and Shaowei Chen*

Department of Chemistry and Biochemistry, University of California, 1156 High Street, Santa Cruz, California 95064

Received June 22, 2010. Revised Manuscript Received August 16, 2010

Janus nanoparticles were prepared by interfacial ligand exchange reactions of octanethiolate-protected gold (AuC8) nanoparticles with 3-mercapto-1,2-propanediol (MPD) at the air/water interface. AFM and TEM measurements showed that the resulting particles formed stable aggregates in water with dimensions up to a few hundred nanometers, in sharp contrast to the original AuC8 particles and bulk-exchange counterparts where the aggregates were markedly smaller. Consistent behaviors were observed in dynamic light scattering measurements. FTIR measurements of solid films of the nanoparticles suggested that the octanethiolate ligands were mostly of trans conformation, whereas the MPD ligands exhibited gauche defects as a consequence of the hydrogen-bonding interactions between the hydroxyl moieties of adjacent ligands. Raman spectroscopic measurements in an aqueous solution of pyridine showed that the pyridine ring breathing modes remained practically unchanged and the intensity profiles indicated minimal interactions between pyridine and the gold cores within the three nanoparticle ensembles. However, water bending vibrational features were found to be enhanced substantially with the addition of Janus nanoparticles, which was ascribed to the formation of clusters of water molecules that were trapped within the nanoparticle ensembles. No apparent enhancement was observed with the AuC8 or bulk-exchange particles.

Introduction

Since Veyssie and co-workers created "Janus beads" by a partial hydrophobic modification of commercial glass spheres,[1,2] "Janus particles" have attracted increasing attention largely because of their unique asymmetrical surface structure, which may be exploited for controlled assembly of the particles into organized ensembles, akin to conventional amphiphilic surfactant molecules. Whereas most earlier studies of Janus particles are focused on polymeric materials with dimensions on the order of a few tens of nanometers to a few micrometers,[3−7] studies of nanometer-sized Janus particles are actually relatively scarce. Such a manipulation of the nanoparticle surface chemistry may be exploited as a powerful variable in the further control of the nanoparticle material properties, in addition to the conventional variables of size and shape. For instance, Hong et al.[8] showed that Janus colloidal spheres (∼1 μm) might form large aggregates by exploiting the opposite electric charge on two hemispheres. Hatton and co-workers[9] demonstrated that, by grafting ionizable polymers onto Janus magnetic nanoparticles (∼20 nm), clustering of the nanoparticles might be induced and controlled by varying solution pH.

Recently, we reported that nanosized Janus particles could be readily prepared by using an interfacial engineering approach where hydrophobic alkanethiolate-protected gold nanoparticles were used as the illustrating examples.[10−13] Experimentally, the gold nanoparticles were spread onto the water surface of a Langmuir−Blodgett trough forming a monolayer at the air/water interface. Upon mechanical compression, ligand intercalation occurred between adjacent nanoparticles such that the interfacial mobility of the nanoparticles was significantly reduced. Hydrophilic ligands were then injected into the water subphase to initiate ligand exchange reactions with the bottom face of the nanoparticles. The resulting particles exhibited hydrophobic character on one face and hydrophilic on the other. Such an amphiphilic structure was confirmed by a variety of experimental measurements including contact angle and AFM adhesion force, as well as NOESY NMR spectroscopic measurements.[10−13]

Because of the asymmetrical surface structure, the resulting Janus nanoparticles behave analogously to conventional surfactant molecules, forming stable aggregates in water. In this paper, we carried out a detailed study to examine the nanoparticle aggregates at varied particle concentrations by AFM, TEM, DLS, FTIR, and Raman spectroscopic measurements. The results were then compared with those of the original hydrophobic nanoparticles and bulk-exchange nanoparticles where the surface ligands were mixed homogenously. From these measurements, the critical micelle concentration of the Janus particles was then estimated.

Experimental Section

Chemicals. Hydrogen tetrachloroauric acid ($HAuCl_4 \cdot xH_2O$) was synthesized by dissolving ultrahigh purity gold (99.999%, Johnson Matthey) in freshly prepared aqua regia followed by crystallization.[14] Tetra-*n*-octylammonium bromide (Alfa Aesar, 98%),

*To whom correspondence should be addressed. E-mail: shaowei@ucsc.edu.

(1) Casagrande, C.; Veyssie, M. *C. R. Acad. Sci., Ser. II* **1988**, *306*, 1423–1425.
(2) Casagrande, C.; Fabre, P.; Raphael, E.; Veyssie, M. *Europhys. Lett.* **1989**, *9*, 251–255.
(3) Perro, A.; Reculusa, S.; Ravaine, S.; Bourgeat-Lami, E. B.; Duguet, E. *J. Mater. Chem.* **2005**, *15*, 3745–3760.
(4) Roh, K. H.; Martin, D. C.; Lahann, J. *Nat. Mater.* **2005**, *4*, 759–763.
(5) Suzuki, D.; Kawaguchi, H. *Colloid Polym. Sci.* **2006**, *284*, 1471–1476.
(6) Nie, Z. H.; Li, W.; Seo, M.; Xu, S. Q.; Kumacheva, E. *J. Am. Chem. Soc.* **2006**, *128*, 9408–9412.
(7) Nisisako, T.; Torii, T.; Takahashi, T.; Takizawa, Y. *Adv. Mater.* **2006**, *18*, 1152–1156.
(8) Hong, L.; Cacciuto, A.; Luijten, E.; Granick, S. *Nano Lett.* **2006**, *6*, 2510–2514.
(9) Lattuada, M.; Hatton, T. A. *J. Am. Chem. Soc.* **2007**, *129*, 12878–12889.
(10) Pradhan, S.; Xu, L. P.; Chen, S. W. *Adv. Funct. Mater.* **2007**, *17*, 2385–2392.
(11) Xu, L. P.; Pradhan, S.; Chen, S. W. *Langmuir* **2007**, *23*, 8544–8548.
(12) Pradhan, S.; Brown, L. E.; Konopelski, J. P.; Chen, S. W. *J. Nanopart. Res.* **2009**, *11*, 1895–1903.
(13) Pradhan, S.; Ghosh, D.; Chen, S. W. *ACS Appl. Mater. Interfaces* **2009**, *1*, 2060–2065.
(14) Brauer, G. *Handbook of preparative inorganic chemistry*, 2nd ed.; Academic Press: New York, 1963.

Scheme 1. Schematics of AuC8, Bulk-Exchange, and Janus Nanoparticles

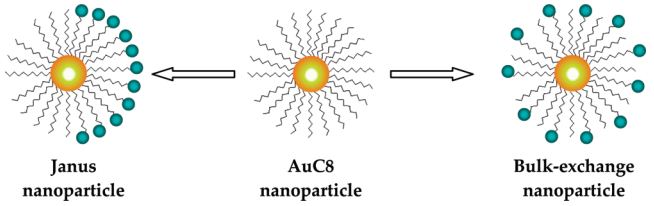

n-octanethiol (C8SH, Acros, 96%), sodium borohydride ($NaBH_4$, Acros, 99%), and 3-mercaptopropane-1,2-diol (MPD, Aldrich, 95%) were all used as received. Solvents were purchased from typical commercial sources at their highest purities and used without further treatments. Water was supplied by a Barnstead Nanopure water system (18.3 MΩ·cm).

Gold Janus Nanoparticles. Gold Janus nanoparticles were prepared by using an interfacial engineering approach based on the Langmuir method, which was detailed previously.[10] Briefly, a monolayer of octanethiolate-protected gold (AuC8) nanoparticles (average core diameter 5.0 nm and core size dispersity ca. 10%, as determined by transmission electron microscopic measurements) was first deposited onto the water surface of a Langmuir−Blodgett trough (NIMA Technology, model 611D).[15−17] The particle monolayer was then compressed to a desired surface pressure where the interparticle edge-to-edge separation was maintained at a value smaller than twice the extended ligand chain length such that the interfacial mobility of the particles was impeded. At this point, a calculated amount of MPD ligands was injected into the water subphase by a Hamilton microliter syringe where interfacial ligand exchange reactions occurred. The resulting particles exhibited hydrophobic character on one face and hydrophilic on the other, analogous to the dual-face Roman god, Janus (Scheme 1). The amphiphilic characters of the Janus nanoparticles were quantified by contact angle measurements (Tantec CAM-PLUS contact angle meter), where the nanoparticle monolayers were transferred onto a clean glass slide surface by either the upstroke or downstroke deposition method. The contact angles were estimated to be $66.2 \pm 2.5°$ and $48.1 \pm 2.7°$, respectively, which were consistent with the results reported previously.[10]

As a control experiment, MPD-functionalized gold nanoparticles were also prepared by exchange reactions where calculated amounts of AuC8 nanoparticles and MPD ligands was codissolved in THF under vigorous magnetic stirring for two days (with the eventual MPD/C8 ratio on the particle surface similar to that of the Janus particles). The solution was then dried by a rotary evaporator at reduced pressure and excessive free ligands were removed by extensive rinsing with ethanol. The resulting particles were denoted as bulk-exchange particles (Scheme 1).

^{1}H NMR measurements showed that for both the Janus and bulk-exchange nanoparticles, the concentration of the MPD ligands on the nanoparticle surface was both close to 50%. That is, these two particles might be considered as structural isomers.[10]

Nanoparticle aggregates. The structural details of the controlled assemblies of the nanoparticles (AuC8, bulk-exchange, and Janus) were examined by AFM and TEM measurements. Experimentally, the nanoparticles were first dissolved in THF. An equal amount of water was then added into the solution and THF was removed by bubbling the solution with ultrahigh-purity nitrogen. The samples for AFM measurements were then prepared by dropcasting the resulting aqueous solution of the nanoparticles onto a freshly cleaved mica surface. Solvent evaporation at room temperature led to the deposition of the nanoparticles onto the mica surface. The topographic images were acquired under ambient conditions with a Molecular Imaging PicoLE SPM instrument in tapping mode. The cantilevers exhibited resonant frequencies between 120 and 190 kHz, force constants of 2.5−8.5 N/m, and a tip apex radius of approximately 10 nm.

The samples for TEM measurements were prepared in a similar fashion by casting a drop of the particle solution onto a 200-mesh holey carbon-coated copper grid. TEM micrographs were acquired with a JEOL-F 200 kV field-emission analytical transmission electron microscope in the Molecular Foundry and the National Center for Electron Microscopy at Lawrence Berkeley National Laboratory.

Spectroscopies. Raman spectroscopic measurements were carried out with a Nicolet Almega XR Dispersive Raman Spectrometer (Laser wavelength 780 nm). A calculated amount of pyridine was added into the aqueous solutions. FTIR measurements were carried out with a Perkin-Elmer FTIR spectrometer (Spectrum One, spectral resolution 4 cm^{-1}) where the samples were prepared by casting the particle solutions onto a NaCl disk. Dynamic light scattering (DLS) measurements were carried out with a Protein Solution *Dynapro* temperature controlled microsampler. The results were reported in terms of % mass.

Results and Discussion

The controlled assembly of the nanoparticles was first examined by atomic force microscopy (AFM) measurements. Figure 1 depicts representative AFM topographs of (A,D) AuC8, (B,E) bulk-exchange, and (C,F) Janus nanoparticles acquired in tapping mode at two different particle concentrations: 0.05 mg/mL (A−C), and 1.0 mg/mL (D−F). There are at least two aspects that warrant attention here. First, it can be seen that apparent aggregation of nanoparticles occurred in all three particle samples at both concentrations. As mentioned earlier, all particles were initially dissolved in THF, and an equal amount of water was then added into the solution, followed by nitrogen bubbling to remove the THF. In essence, the samples for AFM measurements were all prepared from the corresponding aqueous solution of the nanoparticles. For AuC8 nanoparticles (A and C), the formation of particle aggregates is not so surprising, since the particles are hydrophobic and not soluble in water. In fact, experimentally the particles were found to gradually settle down from the solution within a few hours. The images in panels (A) and (D) were acquired with freshly prepared particle solutions in water. Similar phenomena were observed with bulk-exchange nanoparticles (B,E) because of poor solubility of the particles in water (note that only approximately 50% of the hydrophobic octanethiolate ligands were replaced by hydrophilic MPD). In sharp contrast, the Janus nanoparticles remained soluble in water for hours without any apparent difference of the solution color and appearance, despite the formation of rather extensive nanoparticle aggregates.[10] This unusual solution stability may be accounted for by the amphiphilic character of the nanoparticles, which renders the nanoparticles to behave analogously to conventional surfactant molecules. The formation of particle assemblies helps minimize the effective solvation energy of the nanoparticles, most probably by exposing the hydrophilic side of the nanoparticles to the solvent medium. For bulk-exchange nanoparticles, because of the homogeneous mixing of the hydrophobic and hydrophilic ligands,[12,18,19] no preferential arrangement of the nanoparticles can be obtained to minimize the solvation energy.

Second, the size of the nanoparticle aggregates exhibits an apparent difference among the three nanoparticle samples, AuC8 < bulk-exchange < Janus nanoparticles, at both concentrations;

(15) Chen, S. W. *Langmuir* **2001**, *17*, 6664–6668.
(16) Chen, S. W. *Langmuir* **2001**, *17*, 2878–2884.
(17) Chen, S. W. *Adv. Mater.* **2000**, *12*, 186–190.
(18) Singh, C.; Ghorai, P. K.; Horsch, M. A.; Jackson, A. M.; Larson, R. G.; Stellacci, F.; Glotzer, S. C. *Phys. Rev. Lett.* **2007**, *99*, 226106–1.
(19) Centrone, A.; Penzo, E.; Sharma, M.; Myerson, J. W.; Jackson, A. M.; Marzari, N.; Stellacci, F. *Proc. Natl. Acad. Sci. U.S.A.* **2008**, *105*, 9886–9891.

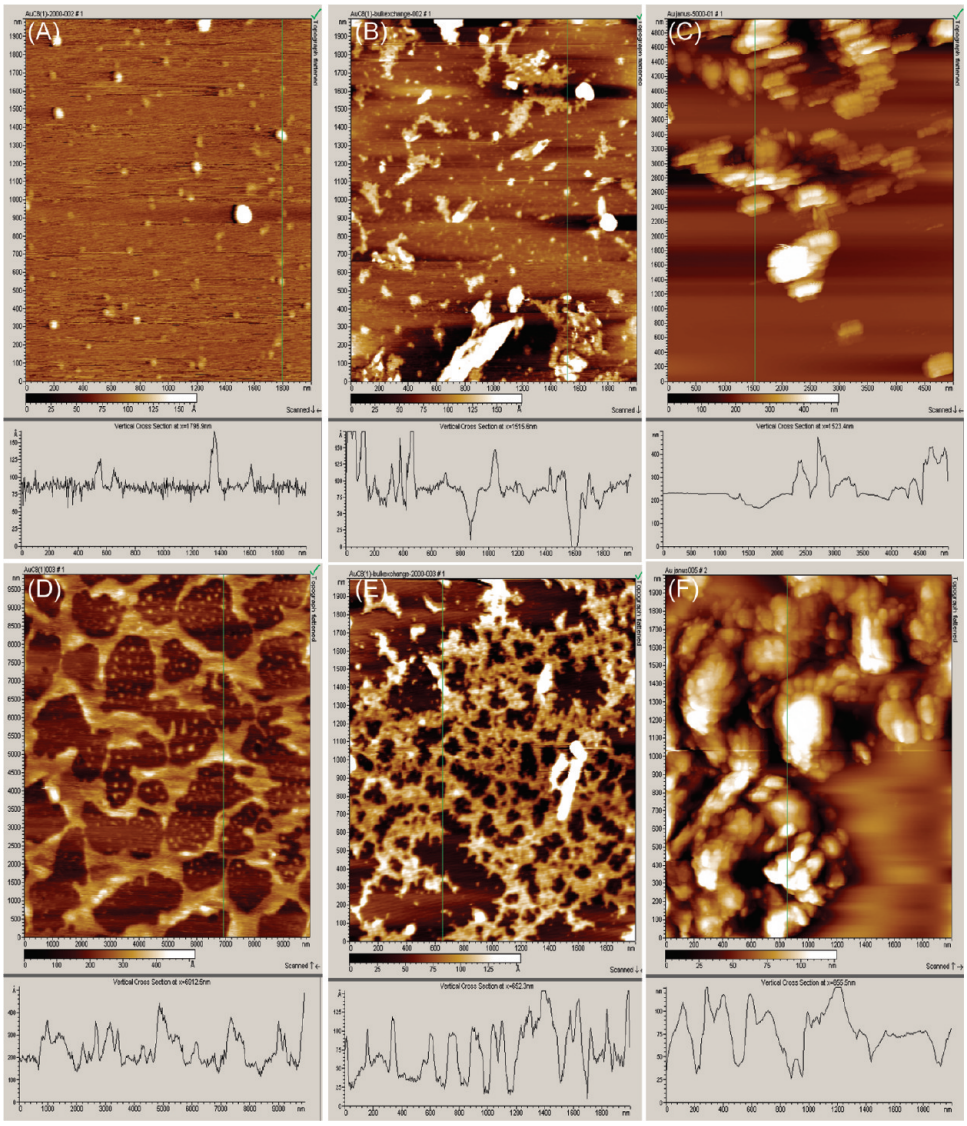

Figure 1. AFM topographs of (A,D) AuC8, (B,E) bulk-exchange, and (C,F) Janus nanoparticles deposited onto a clean mica surface from a solution at either (A,B,C) 0.05 mg/mL or (D,E,F) 1 mg/mL in water. The corresponding line scans are included below each AFM topograph.

and the aggregation became more extensive at higher concentration. Such a discrepancy again can be accounted for by the solubility of the nanoparticles in water. In fact, as AuC8 nanoparticles are not soluble in water, the rapid precipitation of the nanoparticles from the water medium indicates that there was very limited time for the formation of particle aggregates. In other words, the number of nuclei for particle assemblies was large, and consequently, the size of the particle aggregates was small. For instance, at 0.05 mg/mL, a representative line scan shows that the size of the AuC8 particle aggregates (A) was about 7 to 20 nm, corresponding to only a few nanoparticles, on average, within a particle aggregate (note that the physical diameter of an individual nanoparticle was about 7 nm, consisting of the core plus two ligands). In sharp contrast, line scan analysis shows that Janus nanoparticles (C) formed significantly larger particle aggregates, typically on the order of 200 nm. This again may be attributed to the asymmetrical particle surface structure that leads to the formation of superparticulate assemblies, akin to conventional surfactant molecules. For bulk-exchange nanoparticles (B), the size of the nanoparticle aggregates was found to fall in between that of the AuC8 particles and that of the Janus counterparts, within the range of 30 to 80 nm. Consistent behaviors were observed in dynamic light scattering measurements where the hydrodynamic radii of the nanoparticle ensembles increased in the order of AuC8 nanoparticles < bulk-exchange nanoparticles < Janus nanoparticles (Supporting Information Figure S1).

At higher concentrations, all nanoparticle samples exhibited a rather drastic increase of the size of the nanoparticle aggregates. For instance, AuC8 nanoparticles (D) formed a porous network that consisted of nanoparticle aggregates along with individual nanoparticles. The height of the nanoparticle aggregates was 10 to 20 nm and the lateral dimension ranged from a few tens of nanometers to a few hundred nanometers. A similar network structure was also observed with the bulk-exchange nanoparticles (E), although with significantly smaller pores. The height of the particle network was found to be rather uniform, ca. 10 nm, suggesting a single nanoparticle layer. For Janus nanoparticles (F), the aggregation was far more extensive with the height more than 100 nm and the lateral length beyond 1 μm.

The discrepancy among nanoparticle aggregates can also be manifested in TEM measurements. Figure 2 depicts two representative TEM micrographs of the (A) bulk-exchange and (B) Janus nanoparticles that were prepared by drop-casting the corresponding particle solutions in water (1 mg/mL) onto a Cu grid. Again,

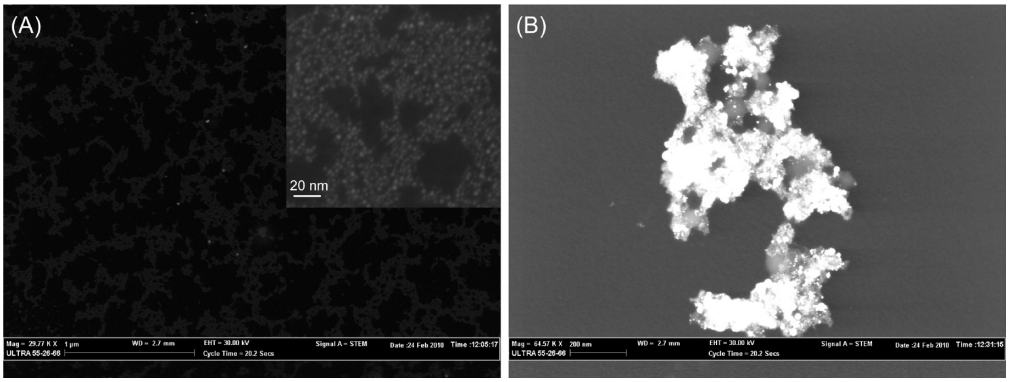

Figure 2. Representative TEM micrographs of (A) bulk-exchange and (B) Janus Au nanoparticles. Samples were prepared by drop-casting the corresponding particle solution in water (1 mg/mL) onto a Cu TEM grid. Scale bars are 1 μm in (A) and 20 nm in the figure inset, and 200 nm in (B).

it can be seen that in panel (A) a porous network structure was formed with the bulk-exchange nanoparticles where the continuous lateral length was extended to the order of micrometers. Furthermore, from the panel inset, one can see that the particle network essentially consisted of a single particle layer. As for the Janus nanoparticles (B), the aggregation is far more extensive, where the nanoparticles essentially formed three-dimensional agglomerates with the dimensions of up to a few hundred nanometers. At lower concentrations, similar nanoparticle aggregates were also observed, although the size decreased accordingly (not shown). Both of these observations are consistent with those from AFM measurements (Figure 1).

One may note that the resulting nanoparticle ensembles exhibited rather irregular morphologies. This may be due to the dispersity of the nanoparticle core size that led to different loading of the hydrophilic ligands on the nanoparticle surface, as suggested in our previous study with AFM adhesion force measurements.[11] Further study with uniform nanoparticles is certainly desired.

Nonetheless, the studies described above suggest that the aggregation/assembly of nanoparticles exhibited sensitive dependence on the nanoparticle surface structures. The amphiphilic nature of Janus nanoparticles affords a unique structural building block where superparticulate ensembles may be constructed and remain stable in solvent media. Further structural details of the nanoparticle assemblies were obtained in spectroscopic measurements. Figure 3 depicts the infrared spectra of the solid films of the three nanoparticle samples. For both the bulk-exchange and Janus nanoparticles, a broad peak can be seen at ca. 3400 cm^{-1}, which may be ascribed to the O-H stretch of the MPD ligands, consistent with the incorporation of the MPD ligands into the nanoparticle surface protecting layer; whereas for the original AuC8 nanoparticles, only a featureless profile appears within this region. Between 2800 and 3000 cm^{-1}, all three nanoparticle samples exhibit two peaks at 2920 and 2852 cm^{-1}, which are attributable to the symmetric (d^+) and antisymmetric (d^-) methylene stretch, respectively.[20] The fact that the energies of these two vibrational stretches are almost identical for the three nanoparticle samples suggests that the partial replacement of the octanethiolate ligands by MPD on the nanoparticle surface (as in bulk-exchange and Janus nanoparticles) did not significantly impact the chain ordering. In fact, the energies are very close to those observed with crystalline polyethylene, signifying the low concentration of gauche defects within the octanethiolate ligands.[20] It should be noted that

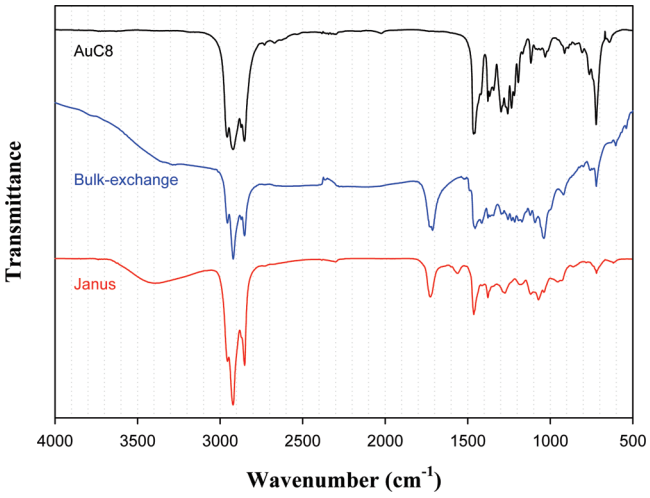

Figure 3. FTIR spectra of solid films of AuC8, bulk-exchange, and Janus nanoparticles.

these two peaks most probably also include contributions from the C−H stretches of the MPD ligands. In fact, Li and co-worker showed that for gold nanoparticles passivated by a full monolayer of MPD ligands the C−H stretches were found at 2918 and 2851 cm^{-1}, as compared to 2931 and 2879 cm^{-1} that are anticipated with monomeric MPD molecules. The observed red-shift was ascribed to the hydrogen bonding interactions between the hydroxyl moieties of adjacent ligands, suggestive of possible gauche conformations of the MPD ligands.

In the low-frequency region, AuC8 nanoparticles exhibited a major band at 721 cm^{-1} and a small one at 641 cm^{-1}. These are assigned to the C−S stretching vibrations with the C−S bond in the trans and cis conformations with the adjacent C−C bond, respectively.[20] In fact, these vibrational features have been exploited as a diagnostic for the orientation of the adjacent C−C bond. The fact that the 721 cm^{-1} peak is substantially more intense than the 641 cm^{-1} one indicates that indeed the ligands on the AuC8 nanoparticle surface are mostly in trans conformation with few defects, consistent with the methylene vibrational properties observed above. Interestingly, with the incorporation of MPD ligands into the particle protecting layer (bulk-exchange and Janus nanoparticles), the intensity of the trans conformer decreases drastically with respect to that of the cis conformer, suggesting the emergence of increasing gauche conformation of the S−C−C linkage that results from the formation of hydrogen-bonding

(20) Hostetler, M. J.; Stokes, J. J.; Murray, R. W. *Langmuir* **1996**, *12*, 3604–3612.

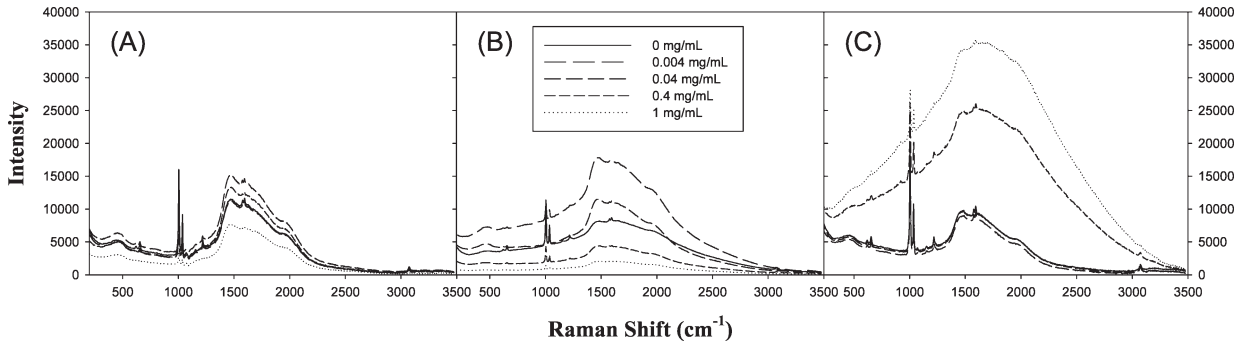

Figure 4. Raman spectra of an aqueous solution of pyridine (pyridine/H_2O, 1:20 v/v) with the addition of varied concentrations of (A) AuC8, (B) bulk-exchange, and (C) Janus nanoparticles, which were shown as figure legends.

interactions between neighboring MPD ligands. Note that the band at 1725 cm^{-1} is most likely due to clusters of water trapped within the particle films (more details below).

The structural characteristics of the nanoparticle assemblies in aqueous solutions were further examined by Raman spectroscopy. Figure 4 depicts the Raman spectra of (A) AuC8, (B) bulk-exchange, and (C) Janus nanoparticles at varied concentrations in a water solution with pyridine (pyridine/H_2O, 1:20 v/v). In all three nanoparticle solutions, two well-defined bands can be seen at 1003 cm^{-1} and 1035 cm^{-1}, which may be assigned to the pyridine ring breathing (ν_1) and ring trigonal (ν_{12}) mode, respectively.[21] One may note that these bands are somewhat blue-shifted as compared to those observed with (neat) liquid pyridine that appear at 993 cm^{-1} and 1032 cm^{-1},[22] but are very comparable to those (1002 cm^{-1} and 1035 cm^{-1}) observed with a water solution containing 0.1 M pyridine and 0.1 M $NaClO_4$.[23] It should be noted that these Raman features appeared even in the absence of any nanoparticles, and the Raman shifts remained virtually unchanged with the addition of different nanoparticles. This observation can be accounted for by the formation of a hydrogen-bonding complex between the nitrogen of the pyridine ring and the hydrogen from the donor molecules (e.g., water and alcohols).[24] In fact, the nature of the hydrogen bonding interactions by pyridine can also be manifested by the ratio of the integrated peak intensity of the two ring vibrational modes, which can be found at $I(\nu_{12})/I(\nu_1) = 0.68 \pm 0.02$ (AuC8), 0.71 ± 0.01 (bulk-exchange), and 0.70 ± 0.02 (Janus), with the addition of the corresponding nanoparticles up to 1 mg/mL. Note that $I(\nu_{12})/I(\nu_1)$ has been exploited as a sensitive parameter to assess the chemical environment of pyridine molecules in solution and on substrate surfaces,[25] where (i) a value of $I(\nu_{12})/I(\nu_1) > 0.65$ typically signifies liquid pyridine, (ii) physisorption of pyridine leads to a smaller ratio of $0.15 < I(\nu_{12})/I(\nu_1) < 0.65$, and (iii) for chemisorbed pyridine, $I(\nu_{12})/I(\nu_1) \approx 0$. The $I(\nu_{12})/I(\nu_1)$ values observed in the present study, while practically unchanged among the series of nanoparticle solutions (and at different particle concentrations), are somewhat smaller than that (0.80) observed with liquid pyridine but larger than that (0.36) of pyridine in water (10% solution), indicative of a chemical environment that is most likely a combined contribution of liquid pyridine and pyridine−water mixtures, and hence the formation of pyridine−H_2O hydrogen bonding networks.[25] Furthermore, the intensity of these pyridine bands exhibited an apparent decrease with increasing nanoparticle concentration, despite the increasingly extensive aggregation of nanoparticles as manifested in AFM and TEM measurements (Figures 1 and 2). One plausible explanation is that the gold nanoparticles (ca. 5 nm in diameter) were too small to produce hot spots within the aggregates for apparent enhancement of the pyridine Raman signals. In fact, in most earlier studies, gold nanoparticles that exhibited apparent surface-enhanced Raman effects were substantially larger (on the order of a few tens of nanometers in diameter).[26−30] Another possible interpretation is that the accessibility of pyridine to the gold cores within the nanoparticle assemblies is limited as a result of the nanoparticle surface-protecting layer, which is consistent with the lack of physisorption or chemisorption of pyridine onto the Au surface.

The lack of surface enhancement of the pyridine Raman features by the nanoparticles is also manifested in the virtually invariant line width of the pyridine ring breathing modes, which was estimated to be approximately 10 cm^{-1} both in the absence and in the presence of varied types of nanoparticles in the solution. This suggests that the interactions between the pyridine and the nanoparticle metal cores are minimal.

Another prominent feature in the Raman spectra is the broad peak ranging from 1300 to 2500 cm^{-1}, which is assigned to the water bending vibrational band. From Figure 4, it can be seen that the intensity of this broad feature exhibits a different variation with the kind of nanoparticles added to the solution. In panel (C), with the addition of up to 0.04 mg/mL Janus nanoparticles, the band intensity remains virtually unchanged. However, a further increase of Janus particle concentration led to a drastic enhancement of the band intensity. For instance, the peak intensity is 36 100 at 1 mg/mL, 25 200 at 0.4 mg/mL, and 9060 at ≤0.04 mg/mL. This enhancement corresponds to the formation of nanoparticle aggregates, as manifested in AFM and TEM measurements. Because of the amphiphilic nature of the nanoparticle surface, the assembly of the Janus nanoparticles most likely resembles that of conventional surfactant molecules with the formation of micelle- or liposome-like structures. Such an orientation helps minimize the solvation energy of the particle ensembles, in which clusters of water may be trapped in between the hydrophilic faces

(21) Mernagh, T. P.; Cooney, R. P.; Spink, J. A. *J. Raman Spectrosc.* **1985**, *16*, 57–61.
(22) http://riodb01.ibase.aist.go.jp/sdbs/cgi-bin/cre_index.cgi?lang=eng.
(23) Wu, D. Y.; Ren, B.; Jiang, Y. X.; Xu, X.; Tian, Z. Q. *J. Phys. Chem. A* **2002**, *106*, 9042–9052.
(24) Fan, H. Y.; Moliva, C. D.; Eliason, J. K.; Olson, J. L.; Green, D. D.; Gealy, M. W.; Ulness, D. J. *Chem. Phys. Lett.* **2009**, *479*, 43–46.
(25) Cooney, R. P.; Mahoney, M. R.; McQuillan, A. J. In *Advances in Infrared and Raman Spectroscopy*; Clark, R. J. H., Hester, R. E., Eds.; Wiley: Heyden, London, 1982; Vol. *9*, pp 188−281.
(26) Wei, A.; Kim, B.; Sadtler, B.; Tripp, S. L. *ChemPhysChem* **2001**, *2*, 743-+.
(27) Joo, S. W. *Vibr. Spectrosc.* **2004**, *34*, 269–272.
(28) Tong, L. M.; Li, Z. P.; Zhu, T.; Xu, H. X.; Liu, Z. F. *J. Phys. Chem. C* **2008**, *112*, 7119–7123.
(29) Ringler, M.; Klar, T. A.; Schwemer, A.; Susha, A. S.; Stehr, J.; Raschke, G.; Funk, S.; Borowski, M.; Nichtl, A.; Kurzinger, K.; Phillips, R. T.; Feldmann, J. *Nano Lett.* **2007**, *7*, 2753–2757.
(30) Chi, H.; Liu, B. H.; Guan, G. J.; Zhang, Z. P.; Han, M. Y. *Analyst* **2010**, *135*, 1070–1075.

of the Janus nanoparticles. With increasing particle concentration, more water clusters are formed within the nanoparticle aggregates. The broad range of the Raman shift is therefore likely due to the dispersity of the size of the water clusters, as theoretical calculations have shown that larger water clusters exhibit greater Raman shifts. For instance, for water clusters larger than a hexamer, additional bending bands start to appear at $>1710\ cm^{-1}$.[31] Importantly, the abrupt change of the Raman band intensity at 0.4 mg/mL might be exploited for the definition of the critical micelle concentration (CMC) of Janus nanoparticles.[32] This cmc (about 0.4 μM) is about 3 orders of magnitude smaller than that for Triton X-100 (0.2 to 0.9 mM).[33−35]

In sharp contrast, the Raman profiles before and after the addition of AuC8 nanoparticles remained almost unchanged with the particle concentration increased from 0 to 1.0 mg/mL (panel A). This is perhaps not surprising, since the nanoparticles are hydrophobic and eventually precipitate out of the solution. It is unlikely that water clusters would be trapped within the particle aggregates. For bulk-exchange nanoparticle (panel B), the behaviors are intermediate between those of the Janus nanoparticles and those of the AuC8 particles. Again, the observed discrepancy in the Raman responses is consistent with the difference of the nanoparticle surface chemistry, which gives rise to distinctly different aggregation structures in solution, as manifested in AFM and TEM measurements (Figures 1 and 2).

Furthermore, one may note that the water stretching mode (typically within the range of 3300 to 3400 cm^{-1}) remains almost invisible even with the addition of any of the three nanoparticle samples into water. This suggests that the enhancement of the bending vibration of the water clusters trapped within the nanoparticle assemblies is markedly higher than that of the stretching mode. In fact, in earlier studies[36] with transition metal electrodes in water, it was found that the interfacial water bending mode exhibited larger enhancement than the stretching one, as a consequence of water adsorption on metal surfaces with the hydrogen end approaching the surface metal atoms when the metal was negatively charged. In the present study, the gold nanoparticles were passivated by a compact monolayer of thiolate ligands. It is thus unlikely that water would be in direct contact with the metallic core. Yet, the hydrogen bonding interactions with the hydroxyl moieties of the MPD ligands are likely responsible for the observed disparity of Raman enhancement between the water bending and stretching modes.

Conclusion

Janus nanoparticles were prepared by an interfacial engineering approach based on ligand exchange reactions. Because of the asymmetrical surface chemistry, the nanoparticles formed stable aggregates in water, analogously to conventional surfactant molecules. This is in sharp contrast to nanoparticles that were passivated by hydrophobic alkanethiolates (AuC8) or nanoparticles with a protecting layer where hydrophobic and hydrophilic ligands were mixed homogeneously (bulk-exchange). AFM and TEM measurements showed that extensive aggregation occurred with Janus nanoparticles, and the dimensions of the aggregates increased with increasing particle concentration. Yet, the degree of aggregation decreased sharply with bulk-exchange particles and became even smaller with the AuC8 particles because of their poor solubility in water. Consistent behaviors were observed in dynamic light scattering measurements. The molecular structures of the particle aggregates were then examined by Raman spectroscopic measurements in a pyridine aqueous solution. The pyridine ring breathing modes were quite consistent among the three types of nanoparticles added to the solution, which suggested limited accessibility of the nanoparticle core surface by pyridine because of the particle protecting monolayer. However, the apparent enhancement of the water bending vibrational intensity with increasing Janus particle concentration indicated that clusters of water molecules might be trapped within the hydrophilic region of the particle aggregates, from which the critical micelle concentration of Janus nanoparticles was estimated to be 0.4 μM. For bulk-exchange and the original AuC8 particles, much smaller changes of the water bending modes were observed, as a result of their energetically unfavored solvation structures in water.

Acknowledgment. We are grateful to the anonymous reviewers for their insightful comments and valuable suggestions. This work was supported in part by the National Science Foundation (DMR-0804049) and ACS-PRF (49137-ND10). TEM work was carried out at the Lawrence Berkeley National Laboratory which is supported by the US Department of Energy.

Supporting Information Available: Dynamic light scattering measurements of the hydrodynamic radii of the nanoparticle ensembles. This material is available free of charge via the Internet at http://pubs.acs.org.

(31) Cybulski, H.; Sadlej, J. *Chem. Phys.* **2007**, *342*, 163–172.

(32) One may note that nanoparticle aggregates started to form at much lower concentrations as shown in Figures 1 and 2. Thus the selection of this concentration as CMC is somewhat arbitrary, but it may represent an upper limit. Experimentally we first prepared the nanoparticles at 1 mg/mL, and then diluted the solutions to varied lower concentrations (0.004 to 0.4 mg/mL). The fact that we observed drastic variation of the dimensions of the nanoparticle aggregates suggests that the nanoparticle aggregates dissembled at concentrations below the CMC value, and the nanoparticle assembly was driven by thermodynamics rather than kinetics, analogous to conventional surfactant molecules.

(33) Liu, M. G.; Cao, C.; Cao, M.; Zhu, C. Q. *Chin. J. Anal. Chem.* **2009**, *37*, 1503–1506.

(34) Valdes-Diaz, G.; Rodriguez-Calvo, S.; Perez-Gramatges, A.; Rapado-Paneque, A.; Fernandez-Lima, F. A.; Ponciano, C. R.; da Silveira, E. F. *J. Colloid Interface Sci.* **2007**, *311*, 253–261.

(35) Ross, S.; Olivier, J. P. *J. Phys. Chem.* **1959**, *63*, 1671–1674.

(36) Wu, D. Y.; Li, J. F.; Ren, B.; Tian, Z. Q. *Chem. Soc. Rev.* **2008**, *37*, 1025–1041.